NMR Relaxation Dispersion Reveals Macrocycle Breathing Dynamics in a Cyclodextrin-based Rotaxane

Shannon Stoffel†, Qi-Wei Zhang§, Dong-Hao Li†, Bradley D. Smith†, Jeffrey W. Peng†,‖,*

†Departments of Chemistry & Biochemistry and ‖Physics, University of Notre Dame, Notre Dame, IN, 46556. §School of Chemistry and Molecular Engineering, East China Normal University, Dongchuan Road 500, Shanghai 200241, China

Corresponding author

Jeffrey W. Peng

Department of Chemistry & Biochemistry

University of Notre Dame

251 Nieuwland Science Hall

Notre Dame, IN 46556

(574) 631-2983 (phone)

(574) 631-6652 (fax)

jpeng@nd.edu

Running Title: NMR Relaxation Dispersion Reveals Rotaxane Macrocycle Breathing

Keywords: Molecular machines | Intercomponent Motion | NMR relaxation dispersion | cyclodextrin | rotaxanes| functional materials |

NMR Relaxation Dispersion Reveals Macrocycle Breathing Dynamics in a Cyclodextrin-based Rotaxane

Shannon Stoffel†, Qi-Wei Zhang§, Dong-Hao Li†, Bradley D. Smith†, Jeffrey W. Peng†,‖,*

†Departments of Chemistry & Biochemistry and ‖Physics, University of Notre Dame, IN 46556, USA. §School of Chemistry and Molecular Engineering, East China Normal University, Dongchuan Road 500, Shanghai 200241, China

Supporting Information Placeholder

ABSTRACT: A distinctive feature of mechanically-interlocked molecules (MIMs) is the relative motion between the mechanically-bonded components, and often it is the functional basis for artificial molecular machines and new functional materials. Optimization of machine or materials performance requires knowledge of the underlying atomic-level mechanisms that control the motion. The field of biomolecular NMR spectroscopy has developed a diverse set of pulse schemes that can characterize molecular dynamics over a broad time scale, but these techniques have not yet been used to characterize the motion within MIMs. This study reports the first observation of NMR relaxation dispersion related to MIM motion. The rotary (pirouette) motion of α-cyclodextrin (αCD) wheels was characterized in a complementary pair of rotaxanes with pirouetting switched ON or OFF. ^{13}C and ^{1}H NMR relaxation dispersion measurements reveal previously unknown exchange dynamics for the αCD wheels in the pirouette-ON rotaxane with a rate constant of 2200 s^{-1} at 298 K, and an activation barrier of $\Delta F^{\ddagger} = 43 \pm 3$ kJ/mole. The exchange dynamics disappear in the pirouette-OFF rotaxane, demonstrating their switchable nature. The ^{13}C and ^{1}H sites exhibiting relaxation dispersion suggest that the exchange involves "macrocycle breathing", in which a αCD wheel fluctuates between a contracted or expanded state, the latter enabling diffusive rotary motion about the axle. The substantial insight from these NMR relaxation dispersion methods suggests similar dynamic NMR methods can illuminate the fast time scale (microsecond-to-millisecond) mechanisms of intercomponent motion in a wide range of MIMs.

INTRODUCTION

Mechanically-interlocked molecules (MIMs) [1-2] are one of the main classes of molecules established by supramolecular chemistry that have enabled the development of artificial molecular machines. Exemplary MIMs include catenanes [3-4] and rotaxanes [5-6]. Both cases involve entangling the topologies of distinct precursor molecules (components) such that they are kept in mutual proximity by a mechanical bond [7]. Critically, two components held together by a mechanical bond can undergo motion relative to one another. Such intercomponent motion, and a means for its control, are the key properties that have enabled MIMs to become the basis for prototype molecular machines.

Rotaxanes are a prominent group of MIMs; they consist of one or more macrocycle components as wheels, threaded by an axle component. Bulky stopper groups at the axle ends keep the macrocycles mounted, while permitting sliding or rotational (pirouetting) motion of the macrocycle relative to the axle. Rotaxanes based on threaded cyclodextrin macrocycles (CD-rotaxanes) [8-10] have been used to demonstrate new modes of switchable intercomponent motion. Examples include the use of redox switching [11-12], and photo-activation [13] to control the shuttling of a CD macrocycle between distinct "stations" along the axle component. Rotaxanes with controlled CD rotational motion about the axle (pirouette motion) have also been developed [14-15].

CD-rotaxanes are also the basis of important new functional materials. These materials consist of poly-CD-rotaxanes – long chain polymers such as polyethylene glycol (PEG) threaded by numerous CD macrocycles [16]. Fusing the CD macrocycles on distinct chains results in molecular "slide-rings" or "slip-link" pulleys that act as mobile interchain crosslinks that allow the PEG chains to slide past one another when there is a mechanical perturbation of the bulk sample [17]. A tangible outcome is a family of "slide-ring" polymer gels, with scratch resistant mechanical properties, that have been incorporated into materials and coatings for the telecommunications industry [18-20].

The applications of CD-rotaxanes as artificial molecular machines or building blocks of functional materials, while obviously distinct, rely on the same basic property: intercomponent motion between the CD wheel and axle components afforded by the mechanical bond. This suggests that the ability to modify intercomponent motion in a predictable manner would

benefit research and development of both molecular machines and materials. Developing that ability requires systematic investigations to disclose the atomic features governing intercomponent motion and its capacity to carry out its intended function.

These considerations motivate the work presented herein: NMR studies of CD rotational motion in a [3]rotaxane recently introduced by Smith and co-workers [15] (**Figure 1**). The [3]rotaxane consists of two "head-to-head" alpha-cyclodextrin (αCD) wheels that can rotate (pirouette) about the threading axle. The pirouette motion is switchable; that is, the [3]rotaxane can be prepared as a pure sample in the pirouette-ON state where pirouetting is allowed. But a sample can be completely switched by chemical treatment to the [1]rotaxane pirouette-OFF state, in which pirouetting is prevented by covalent boronate ester bonds between the axle and wheel components. The switchable pirouetting of these CD-rotaxanes, the first of their kind, makes them attractive as separate but comparable systems for investigating the atomic-level determinants of pirouette motion.

NMR spectroscopy is appealing for these investigations, as it can describe molecular dynamics site-specifically and non-invasively [21]. Thus far, NMR studies of intercomponent motion have consisted mostly of venerable ^{1}H-based methods that are sensitive to motions on the 10-100 ms time-scale. These include traditional ^{1}H 1-D lineshape analyses [22-23] and exchange-mediated transfer of non-equilibrium spin polarization using either 1-D methods [24-25] or 2-D methods, such as EXSY [26]. For example, in the first study of the CD-rotaxanes of **Figure 1** [15], the onset of αCD rotary motion was apparent from the differences in their 1-D ^{1}H lineshapes [15]. These methods are unequivocally effective; nevertheless, they are limited to motions on the 10 – 100 ms time scale [27-28]. In the general case, they are unlikely to cover the range of time scales relevant for intercomponent motion.

Exploring motion over a broad time scale has been and remains a longstanding priority for NMR investigations of biological macromolecules.[27, 29] As a result, there is now a diverse array of NMR pulse schemes to probe motion on time scales that complement ^{1}H lineshape analysis. A particularly prominent example is the family of experiments measuring transverse relaxation dispersion of ^{1}H and heteronuclei (^{13}C, ^{15}N, ^{19}F, ^{31}P). These experiments characterize motions on the 0.1 to 10 ms time scale by measuring spin relaxation rate constants in the presence of an applied radio-frequency (rf) spin-lock [27, 29]. Notably, these experiments can characterize infrequently sampled configurations that are otherwise unobservable. Relaxation dispersion studies have exposed functional motions in both protein and RNA [30], and investigated flexibility-activity relationships for small molecule protein inhibitors and chemical probes [31].

NMR relaxation dispersion measurements would seem to be similarly useful for MIMs. Accordingly, we performed natural abundance ^{13}C and ^{1}H relaxation dispersion studies of the pirouette ON/OFF αCD-rotaxanes in **Figure 1**, and report our results below. In brief, the dispersion studies reveal αCD macrocycle dynamics on the sub-millisecond time scale that are complementary to, yet inaccessible from, the original ^{1}H lineshape data [15]. The results suggest αCD pirouetting is coupled to "macrocycle breathing" – transient expansion of the macrocycle cavity that promotes αCD pirouette motion about the axle.

To our knowledge, this is the first application of NMR relaxation dispersion as a readily available experimental

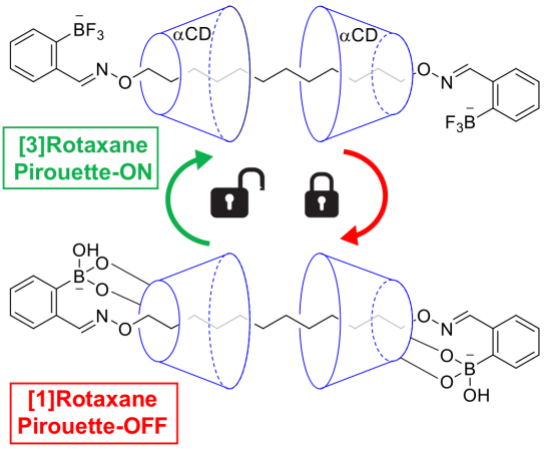

Figure 1. The two separate rotaxanes of this study**. Top**: [3]Rotaxane, pirouette-ON state; **Bottom**: [1]Rotaxane, pirouette-OFF state.

tool to characterize the internal molecular dynamics within a MIM, in this case, a CD-rotaxane. Our findings suggest that similar "flexibility-function profiles" by NMR could be useful for disclosing the mechanisms of intercomponent motion in many other types of MIMs. Our results also underscore the advantage of measuring multiple, and complementary NMR parameters to uncover functional motions that would otherwise elude a single technique.

RESULTS

Indicators of chemical exchange dynamics. We compared the [1] and [3]rotaxanes (pirouette-OFF and -ON states, respectively) using NMR ^{13}C (natural abundance) and ^{1}H spin relaxation measurements. The two rotaxanes were synthesized as described previously [15] and separate samples of each pure rotaxane were prepared for NMR as ~ 4.4 mM solutions, using deuterated DMSO solvent. The NMR spectra were recorded on Bruker Avance I (16.4T) and Avance II (18.8 T) systems, equipped with TCI cryogenically-cooled probes (Bruker Biospin, Inc.). The sample temperatures were 298K (nominal temperature of 303K) unless otherwise stated. Further data acquisition details are in the **Supporting Information**.

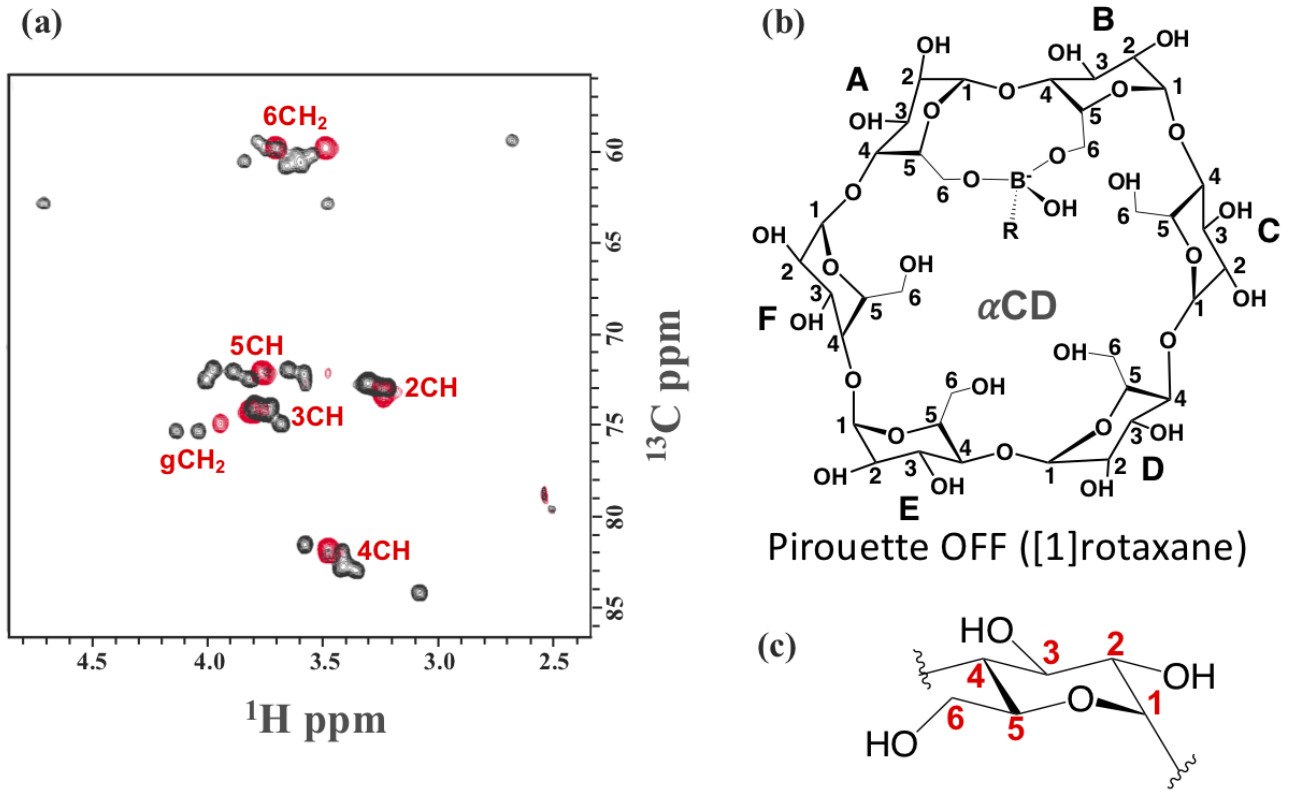

Figure 2. (**a**) Overlay of natural abundance 2-D ^{13}C-^{1}H HSQC spectra (16.4T, DMSO-d6, 298K) of pirouette-OFF [1]rotaxane (**Black**) and Pirouette-ON [3]rotaxane (**Red**). The 2-D cross-peaks indicate methine and methylene ^{13}C-^{1}H bonds of the six glucopyranose residues comprising the αCD wheels. (**b**) Chemical structure of one of the two αCD wheels in the pirouette-OFF [1]rotaxane, viewed along the axle axis, showing the boronate ester linkage via C6 of two adjacent glucopyranose units. (**c**) Chemical structure and carbon atom labels for one of the six glucopyranose units within αCD macrocycle.

The pirouette-ON/OFF states showed clear differences in their NMR spectra indicating differing extents of internal motion. An example is an overlay of their 2-D ^{13}C-^{1}H cross-peaks representing the methine ^{13}C-^{1}H bonds within the αCD glucopyranose units (carbons C2 through C6) (**Figure 2**). Whereas the pirouette-ON ([3]rotaxane) only showed a single set of ^{13}C-^{1}H cross peaks for the chemically distinct carbons in a single glucopyranose unit, the pirouette-OFF ([1]rotaxane) showed a substantially larger number of ^{13}C-^{1}H cross peaks, indicating location-specific chemical shifts for each ^{13}C-^{1}H bond (e.g. C2), and thus, chemical non-equivalence of each of the six αCD glucopyranose units (A through F). Evidently, these non-equivalencies vanish in the pirouette-ON ([3]rotaxane).

These spectral differences indicate ^{13}C chemical exchange processes that are present in the ON state ([3]rotaxane) and absent in the OFF state ([1]rotaxane). We reasoned that the absence of boronate ester bonds in ON state could allow for motions in which the glucopyranose ^{13}C-^{1}H bonds exchanged between states with non-equivalent chemical shifts. Exchange rate constants greater than or equal to the span of non-equivalent chemical shifts (in Hertz) would cause the otherwise distinct ^{13}C-^{1}H cross-peaks from the nonequivalent states to collapse into a single, exchange-averaged cross-peaks located at exchange-averaged chemical shifts [32].

To explore this exchange hypothesis, we conducted natural abundance ^{13}C and ^{1}H NMR relaxation dispersion experiments [33-34]. These experiments are ideal for studying exchanging nuclear spins that yield only single observable resonance. They exploit the fact that the relaxation properties of exchanging nuclei (spins) retain information concerning the transiently sampled states rendered "invisible" by excessive line-

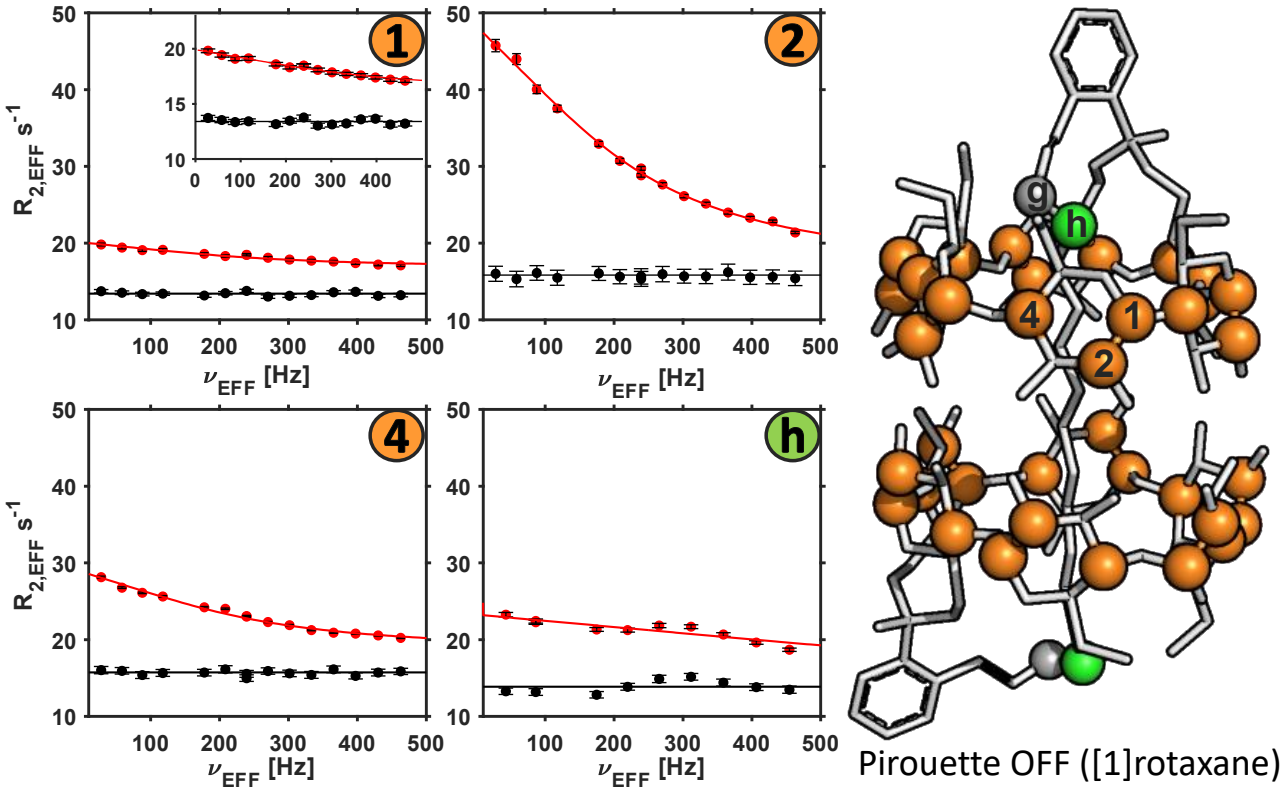

Figure 3: ^{13}C natural abundance CPMG $R_{2,EFF}$ versus ν_{EFF} (28 to 463 Hertz) at 16.4 T in DMSO-d6 for αCD glucopyranose carbons C1, C2, and C4 (290K) and axle methylene carbon 'h' (298K) for the pirouette-ON ([3]rotaxane) (**red**) and pirouette-OFF ([1]rotaxane)(**black**) states. The pirouette-ON ([3]rotaxane) carbons showed dispersion responses that fit to a global, two-state exchange model (red traces) per **Table 1**. The pirouette-OFF carbons showed flat responses (no dispersion) and the black horizontal lines indicate their average $R_{2,EFF}$. The inset in the C1 profile expands the vertical axis to show the presence versus absence of dispersion in the pirouette-ON and OFF states, respectively. The locations of the four types of carbon are shown in the molecular model of pirouette-OFF ([1]rotaxane). Orange spheres are glucopyranose carbons with C1, C2, and C4 labeled. The gray 'g' and green 'h' spheres are axle methylene carbons.

broadening, lopsided populations, or both [35]. "Dispersion" refers to the dependence of the spin relaxation rate constants on the strength of an applied radio-frequency (rf) spin-lock. Importantly, the observed frequency-dependence is a function of the exchange rate constants, the chemical shift differences between exchange-coupled states, and their equilibrium populations. In favorable situations, all three types of information can be estimated from the experimental data [34-39]. We conducted these dispersion measurements for the pirouette-ON/OFF states, as described below, for both ^{13}C and ^{1}H nuclei.

^{13}C relaxation dispersion studies. We performed rotaxane ^{13}C dispersion studies at natural abundance using 2-D heteronuclear pulse-schemes described previously [31, 40]. These schemes measure an effective ^{13}C transverse relaxation rate constant, $R_{2,EFF}$, during a relaxation-compensated Carr-Purcell-Meiboom-Gill (CPMG) spin-lock – a train of ^{13}C 180$_0$ refocusing pulses with an interpulse delay t_{CP}, corresponding to an rf-field strength in Hertz of $\nu_{EFF} = 1/2\ t_{CP}$. The dispersion experiments produce profiles of $R_{2,EFF}$ of versus $\nu_{EFF} = 1/2\ t_{CP}$ for the exchanging nuclei. The profile shape is sensitive to exchange processes with rate constants $k_{EX} < 2\ \pi\ \nu_{EFF,MAX}$ [39, 41].

We collected the ^{13}C dispersion data by recording a series of 2-D^{13}C-^{1}H spectra with a fixed CPMG spin lock length T_{RELAX} but variable rf-field strengths, $\nu_{EFF} = 1/2\ t_{CP}$, with ν_{EFF} sampling values from 28 Hz to 463 Hz. The resulting series of 2-D ^{13}C-^{1}H cross peaks were the raw data for determining site-specific ^{13}C $R_{2,EFF}$ versus ν_{EFF} profiles for the pirouette-ON/OFF states. Critically, profiles showing dispersion ($R_{2,EFF}$ decreasing with increasing ν_{EFF}) identified the ^{13}C sites undergoing exchange. Flat-profiles indicated either an absence of exchange, or exchange processes with rate constant $> 2\ \pi\ \nu_{EFF,MAX}$.

We determined ^{13}C $R_{2,EFF}$ versus ν_{EFF} profiles for the methine glucopyranose carbons C1-C5, and the methylene C6. The C3, C5, and C6 showed flat profiles (Supporting Information**, Figure S1**). By contrast, C1, C2, and C4 showed significant dispersion ($R_{2,EFF}$ decreasing at larger ν_{EFF}) in the pirouette-ON state

([3]rotaxane) indicating exchange dynamics at these carbons (red traces, **Figure 3**). These same C1, C2, and C4 carbons showed flat profiles in the pirouette-OFF state (black traces), indicating no dispersion. Thus, fusing the axle to the αCD wheels via the boronate ester bonds quashed the αCD ^{13}C exchange dynamics of the ON state. Such quashing reveals the switchable nature of the dispersion-detected ^{13}C exchange dynamics.

It is noteworthy that the C1, C2, and C4 carbons showing switchable exchange dynamics are located away from the boronate-ester bonds responsible for the ON to OFF switching. Specifically, the boronate ester bonds attach to C6 of glucopyranose residues A and B, respectively (**Figure 2**, panel (**b**), labeled atoms). Those attachment points bracket just one out of six glycosidic linkages defining each αCD wheel; nevertheless, they affect the entire αCD wheel. This propagated behavior, reminiscent of protein allostery, suggests that the dispersion-derived exchange reflects some collective motion of the αCD wheels in the pirouette-ON state.

Our dispersion measurements of the axle methylene units (^{13}C-$^{1}H_2$) were limited to just the 'g' and 'h' axle carbons by cross-peak overlap. The 'g' methylene carbon lacked dispersion (flat response) for both pirouette-OFF and ON states. By contrast, the 'h' methylene carbon showed modest but significant dispersion in the pirouette-ON state that vanished in the pirouette-OFF state (**Figure 3**). Thus, the axle component also showed evidence of switchable ^{13}C exchange dynamics.

In general, $R_{2,EFF}$ reflects the sum $R_{2,EFF}(\nu_{EFF}) = R_{EX}(\nu_{EFF}) + R_{2,NE}$, where $R_{EX}(\nu_{EFF})$ is the frequency-dependent relaxation due to the micro-millisecond exchange dynamics of interest, and $R_{2,NE}$ is a frequency-independent "plateau" value due to non-exchange mechanisms. Thus, before fitting the experimental dispersion profiles (*vide infra*), we needed to investigate the extent to which differences between the ON versus OFF ^{13}C $R_{2,EFF}$ values might reflect differences in $R_{2,NE}$. The $R_{2,NE}$ relaxation mechanisms include heteronuclear dipole-dipole and chemical shift anisotropy mechanisms modulated by overall molecular tumbling with a correlation time, τ_{ROT} , which is typically on the order of nanoseconds. We therefore wanted to compare τ_{ROT} for the pirouette OFF and ON states to check for possible differences in R2,NE.

To estimate τ_{ROT}, we measured laboratory-frame ^{13}C $R_2=1/T_2$ and $R_1=1/T_1$ relaxation rate constants for the αCD glucopyranose methines of the same samples and static magnetic field strengths, using established 2-D ^{13}C-^{1}H methods [42-43]. Analysis of the methine ^{13}C R_2/R_1 ratios [43] gave us τ_{ROT} estimates, which turned out to be the same for pirouette-ON/OFF states, within the estimated errors (τ_{ROT} = 2.7 ± 0.2 ns/r).

To independently confirm our measurements, we estimated τ_{ROT} via a different approach, measurement of

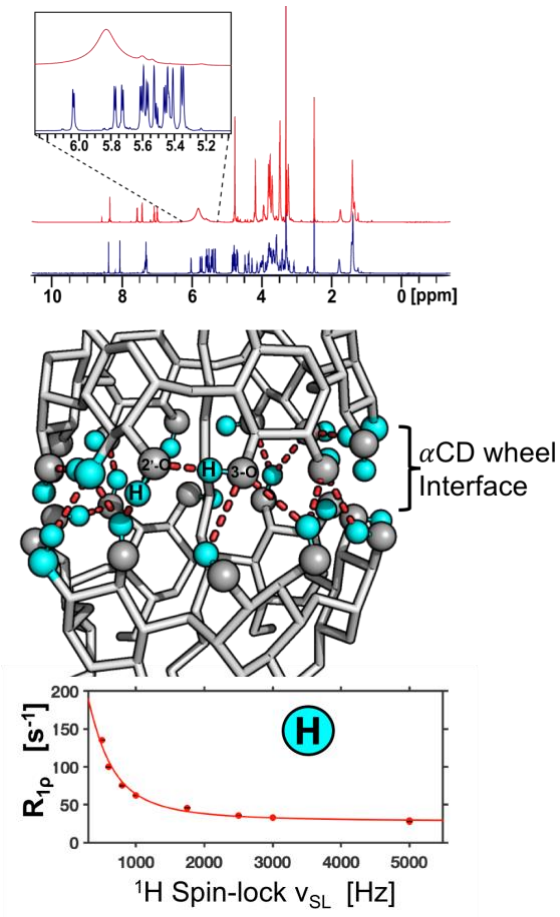

Figure 4. (**Top**) Line-broadening of glucopyranose 2-O_1H/3-O_1H protons at 5 ~ 5.8 ppm in the Pirouette-ON [3]rotaxane (**red**) versus the Pirouette-OFF [1]rotaxane (**blue**). (**Middle**) The hydrogen atoms (cyan spheres) can mediate both intra-wheel and inter-wheel hydrogen bonds. (**Bottom**) On-resonance ^{1}H $R_{1\rho}$ profile for 2-O_1H/3-O_1H protons at 16.4T, T = 298K, DMSO-d6.

the translational diffusion coefficients, D_{TRANS}, using Diffusion Ordered Spectroscopy (DOSY) experiments [44](Supporting Information, **Figure S2**). We related the experimental D_{TRANS} values to $D_{ROT} = 1/6\tau_{ROT}$ the rotational diffusion coefficient, using the Stokes drag coefficients for translation and rotational diffusion of a sphere [45]. Within the estimated errors, the pirouette-ON/OFF states gave the same D_{TRANS} values (0.98 ± 0.01 x 10^{-10} m^2 s^{-1}) and corresponding τ_{ROT} values (2.8 ± 0.03 r/s). Moreover, these DOSY-derived τ_{ROT} values were within the statistical errors estimated from the ^{13}C R_2/R_1 ratios.

We conclude that τ_{ROT}, the correlation time for overall tumbling, is essentially the same for the pirouette-OFF/ON rotaxanes. Thus, we can confidently attribute the differences in $R_{2,EFF}$ for the pirouette-ON/OFF states (**Figure 3**) to differences in exchange dynamics.

^{1}H relaxation dispersion studies. The pirouette-ON/OFF systems also exhibit marked differences in their 1-D ^{1}H spectra (**Figure 4**). The pirouette-OFF state

([1]rotaxane) showed distinct 3-O$_1$H/2-O$_1$H hydroxyl proton resonances for the αCD glucopyranosyl residues, whereas the pirouette-ON state ([3]rotaxane) showed only a broad "hump", at ~ 5.86 ppm with an apparent linewidth (FWHM) of ~ 100 Hz (16.4T, 298K). These differences suggested switchable exchange dynamics affecting the 3-O$_1$H/2-O$_1$H chemical shifts.

We investigated this possibility via 1-D rotating-frame $R_{1\rho}=1/T_{1\rho}$ relaxation dispersion experiments for the 3-O$_1$H/2-O$_1$H hydroxyl protons in the pirouette-ON/OFF states. $R_{1\rho}$ is the rate constant for the relaxation of magnetization along the direction of an applied continuous wave (CW) spin-lock. The dispersion experiments measure the dependence of $R_{1\rho}$ on the effective rf-field strength of the spin-lock, ν_{SL} [33-34]. Spins undergoing chemical exchange show a characteristic decrease of $R_{1\rho}$ with increasing ν_{SL}, analogous to the decrease of the CPMG ^{13}C $R_{2,EFF}$ with ν_{EFF}. To selectively excite the hydroxyl protons, we applied an e-PHOGSY spin echo [46-47] just prior to the spin-lock. The results consisted of $R_{1\rho}$ versus ν_{SL} (100 to 4800 Hz) in **Figure 4**. The pirouette-ON state displayed a clear ^{1}H dispersion profile for the 3-O$_1$H/2-O$_1$H hump; by contrast, the 6-O$_1$H hydroxyl protons did not. The pirouette-OFF state lacked any evidence of $R_{1\rho}$ dispersion. Thus, like the carbon C1, C2, and C4 nuclei, the 3-O$_1$H/2-O$_1$H nuclei exhibited switchable exchange dynamics.

Exchange parameters from the dispersion data. The atomic sites showing relaxation dispersion in **Figures 3**, **4** – that is, ^{13}C $R_{2,EFF}$ or O$_1$H $R_{1\rho}$ decreasing with increasing ν_{EFF} or ν_{SL} – correspond to ^{13}C (C1, C2, and C4) or hydroxyl O$_1$H (3-O$_1$H, 2-O$_1$H) nuclei exchanging between states with non-equivalent isotropic chemical shifts. Here, the word "state" means a subpopulation of the molecule's equilibrium ensemble yielding the same isotropic chemical shift for a given nuclear spin. The exchange of a nucleus between states with non-equivalent chemical shifts causes its local chemical shielding to act like a stochastic magnetic field, which amplifies transverse relaxation (exchange broadening).

The shapes of the dispersion profiles depend on the microscopic details of the exchange dynamics. Fitting those shapes to model functions yields dynamic information including exchange rate constants, fractional populations of the exchange-coupled states, and the corresponding span of chemical shifts [33, 37-38].

We used model functions appropriate for CPMG [38] and $R_{1\rho}$ [48]relaxation (Supporting Information, **Eqs S2-S5**). The model functions assume the simplest case of a two-state exchange process, in which the ^{13}C or ^{1}H spins exchange between just two states (e.g. A ← → B) with distinct chemical shifts. In both cases, the adjustable parameters were: (**i**) the net exchange rate constant, k_{EX} = k(A->B) + k(B->A) (τ_{EX} = 1/k_{EX} is the effective correlation time for the exchange process); (**ii**) the minor state fractional population, P_{MIN} (the other immediately determined by 1 – P_{MIN}); (**iii**), the magnitude chemical shift difference between the two putative states $|\delta\omega_{AB}|$(rad/sec); (**iv**) and $R_{2,NE}$, the non-exchange relaxation contribution.

TABLE 1. [3]Rotaxane: ^{13}C CPMG Dispersion Two-State Exchange Parameters, 16.4 T, d6-DMSO, 4.3mM

T/K	Site	k_{EX} (r/s)	P_{MIN}	Δ_{ppm}	R_{NE} (s-1)
290	C1	1450±30	0.50± 0.13	0.124± 0.002	16.83 ±0.36
	C2	1450±30	0.50± 0.13	0.382± 0.004	16.77± 0.17
	C4	1450±30	0.50± 0.13	0.218± 0.002	18.77± 0.07
298	C1	2200 ± 70	0.46 ± 0.24	0.117± 0.003	13.62± 0.05
	C2	2200 ± 70	0.46 ± 0.24	0.336± 0.001	15.48± 0.05
	C4	2200 ± 70	0.46 ± 0.24	0.198± 0.001	15.71± 0.02
	h	5234 ± 20	0.36 ± 0.01	0.443± 0.002	12.68± 0.13
303	C1	3110± 130	0.50 ± 0.04	0.141± 0.010	11.96± 0.05
	C2	3110± 130	0.50 ± 0.04	0.322± 0.017	13.97± 0.01
	C4	3110± 130	0.50 ± 0.04	0.201± 0.012	13.74± 0.05

We found that the ON-state ^{13}C methine C1, C2, and C4 dispersion profiles were amenable to a global two-state fit; that is, they could be simultaneously fit to same k_{EX}, and fractional population P_{MIN}. The other fitting parameters, $\delta\omega_{AB}$ and $R_{2,NE}$, remained site-specific. The global fit suggested a

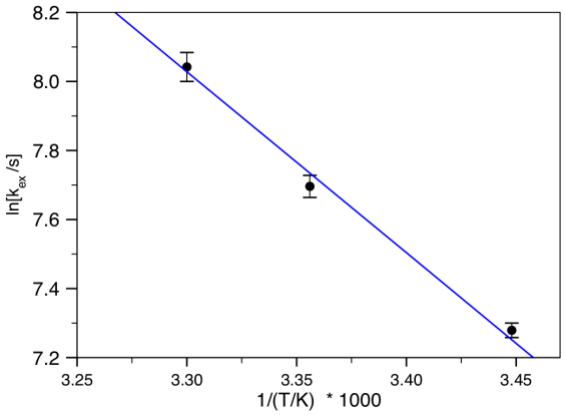

Figure 5. Temperature dependence of k_{EX} based on relaxation dispersion of ^{13}C-^{1}H methines of the pirouette-ON state ([3]Rotaxane). The slope yields an activation barrier $\Delta F^{\ddagger}$ = 43 ± 3 kJ/mol (~ 17± 1 k_BT_R).

collective process affecting the entire αCD wheel (see **Table 1**).

By contrast, the ^{13}C methylene dispersion profile for the axle 'h' carbon converged to a larger k_{EX} that was incompatible with the global C1-C2-C4 fit. Thus, while the 'h' carbon demonstrated switchable exchange dynamics, they appear distinct from those of the αCD methines. This is not unexpected, as the axle and wheel are distinct components in the [3]rotaxane that are not connected by a covalent bond.

We then fit the 3-O_1H/2-O_1H $R_{1\rho}$ versus ν_{SL} profile to a two-state model appropriate for CW spin-locking [48]. Interestingly, the ^1H $R_{1\rho}$ dispersion fits at 290K and 298K gave k_{EX} and P_{MIN} values quite close to those obtained from the C1-C2-C4 global fit (**Table 2**). In particular, fitting the O_1H $R_{1\rho}$ dispersion profiles with k_{EX} and P_{MIN} held at values from the ^{13}C C1-C2-C4 global fit produced negligible change (< 1%) in the $R_{1\rho}$ chi-squared value (sum of squared errors). At 303K, the agreement decreased; the same "cross-fitting" procedure caused a 13% increase in the ^1H $R_{1\rho}$ chi-squared error. Nevertheless, their optimal values remain close. This unexpected closeness suggests that a common dynamic process modulates both the 3-O_1H/2-O_1H and ^{13}C methine chemical shifts.

TABLE 2. [3]Rotaxane: Hydroxyl ^1H $R_{1\rho}$ Dispersion Two-State Exchange Parameters, 16.4 T, d6-DMSO, 4.3mM

T /K	k_{EX} (r/s)	P_{MIN}	Δ_{ppm}	R_{NE} (s^{-1})
290	1480± 140	0.50 ± 0.06	0.48 ± 0.04	28.2 ± 0.4
298	1630± 650	0.50 ± 0.16	0.54 ± 0.07	26.9 ± 0.9
303	2500± 550	0.50 ± 0.13	0.46 ± 0.04	20.4 ± 0.8

Temperature dependence of the exchange process. We explored the temperature dependence of k_{EX} by repeating the ^{13}C methine and 3-O_1H/2-O_1H dispersion experiments at two additional temperatures (Supporting Information, **Figure S3**). Assuming a simple exponential dependence [49], we plotted ln(k_{EX}•s) versus the reciprocal temperature (1/T) to estimate the activation barrier. The slope estimated a free energy barrier of $\Delta F^{\ddagger} = 43 \pm 3$ kJ/mole (~ 17.4 k_BT_R) (**Figure 5**). This value is slightly high compared to hydrogen-bonds in H_2O solvent (~10 k_BT_R) , and somewhat less than those reported for DMSO-water hydrogen bonds [50].

DISCUSSION

The mechanically-interlocked molecules (MIMs) in **Figure 1** are rare examples of structurally related αCD-rotaxanes with rotary pirouette motion completely switched ON or OFF [15]. As such, they present an opportunity to identify critical features regulating such motion that could provide a basis for structural control. A quantitative site-resolved description of intercomponent motion was obtained from ^{13}C and ^1H NMR relaxation dispersion measurements. It is important to emphasize that the dispersion experiments explore motional time scales (0.1 to 1 millisecond) that are distinct from those probed by ^1H lineshape analyses (10 to 100 milliseconds) or ^1H-^1H EXSY (1-100 milliseconds) common in studies of MIM motion [5, 51-56].

The dispersion measurements revealed clear evidence of exchange dynamics for the two αCD macrocycles in the pirouette-ON state ([3]rotaxane). In particular, several glucopyranose carbons displayed ^{13}C $R_{2,CPMG}$ dispersion, including: **i**) C1 and C4, carbons bracketing the α−1,4-glycosidic linkages between adjacent glucopyranose residues; **ii**) and C2, which has a side chain hydroxyl, 2-O_1H, located at the interface between the two αCD wheels. In fact, the 2-O-^1H and 3-O-^1H protons, which both reside in the inter-wheel space, showed significant ^1H $R_{1\rho}$ dispersion. Fits of the experimental ^{13}C and ^1H dispersion profiles to two-state model functions at three temperatures produced exchange rate constants and fractional populations that were strikingly similar (**Table 1**). This strongly suggests a common dynamic process underlying both the ^{13}C and ^1H dispersion profiles – a mode of collective motion for the αCD wheels with an effective two-state rate constant k_{EX} = 2200 s^{-1} at room temperature (298 K).

Importantly, the exchange dynamics are switchable: the ^{13}C and ^1H dispersion in the pirouette-ON state ([3]rotaxane) vanish in the pirouette-OFF state ([1]rotaxane). The OFF state is enforced by boronate ester bonds that covalently fuse each axle end to its proximal αCD wheel. The boronate ester bonds are linked via C6 carbons on two adjacent glucopyranose units within the αCD macrocycle (**Figure 1**). These local attachments have global consequences: quenched exchange at distinct carbon (C1, C2, and C4) and hydroxyl proton (2-O_1H, 3-O_1H) sites around the entire αCD macrocycle. This behavior is reminiscent of the allosteric responses of coupled subunits engaged in long-range, collective motion; localized perturbation at one subunit can propagate to other subunits [57-59].

By themselves, the relaxation dispersion observations do not identify specific configurational dynamics. Instead, their physical basis (stochastic modulation of isotropic chemical shifts caused by exchange dynamics) guides our consideration of plausible rotaxane motions. In particular, such motions should: **i**) modulate those physicochemical properties producing the site-specific variations in the ^{13}C and hydroxyl ^1H chemical shifts; **ii**) reduce sharply upon formation of the boronate ester bonds that turn off the pirouette motion.

Chemical shift modulation and pirouette-ON motion. There is substantial literature showing the dependence of αCD glycosidic C1 and C4 ^{13}C chemical

shifts on the intervening glycosidic torsion angles ϕ, ψ. [60-63] Solid-state CP/MAS NMR studies of crystalline αCD samples [62] with corresponding x-ray crystal structures[64-65] revealed that the breadth of solid-state C1, C4 chemical shifts is indicative of the breadth of ϕ, ψ around the αCD macrocycle. For example, cavity-vacant versus cavity-occupied αCD produced C1 shifts with an rmsd of 1.8 ppm versus 0.27 ppm, respectively. Notably, the span of ϕ, ψ values in the cavity-vacant crystal structure was broader and included outlying ϕ, ψ values stabilized by hydrogen bonds considered unrepresentative of the solution state [62] The rsmd of cavity-occupied αCD (0.27 ppm) compares well with the pirouette-ON Δ_{ppm} values obtained from ^{13}C dispersion studies (Δ_{ppm} = 0.1 to 0.4 ppm in **Table 1**), likely a reflection of the fact that the rotaxane αCDs are cavity-occupied by the axle. In total, our pirouette-ON Δ_{ppm} values are comparable with the lower range of solid-state C1 and C4 shifts attributed to ϕ, ψ variability of the αCD macrocycle.

Another indication that the dispersion-derived ^{13}C Δ_{ppm} reflect torsion angle variation is the spread of C1 and C4 shifts observed for the pirouette-OFF state ([1]rotaxane) [15]. As a result of the boronate ester linkages, the glucopyranose ^{13}C and ^{1}H shifts from different residues are resolved. The C1, C2, and C4 show rmsd values of 0.39, 0.11, and 0.57 ppm; these values exclude the carbons from the two glucopyranose residues that bridge to the boronate esters.

Computational approaches have revealed the sensitivity of solution-state ^{13}C shifts to αCD ϕ, ψ fluctuations. Specifically, Moyna and co-workers developed *ab initio* ^{13}C chemical shift surfaces capable of reproducing the C1 and C4 variations in the solid-state studies described above. Applying those surfaces to αCD conformers sampled by a 5 ns molecular dynamics simulation in water reproduced the solution-state C1 and C4 shifts, and established them as averages over broad distribution of ψ values (ψ_{MIN} = -51.4, ψ_{MAX} = 109.4, ψ_{AVG} = 7.3 +/± 15.3 deg) [66-67] Critically, the breadth of ψ values overlapped well with the ψ distribution determined by the NMR study of Thaning *et al*. [68], the latter revealing two preferred regions of ψ, suggesting at least two macrocycle conformations in equilibrium exchange. Finally, a recently reported 5-microsecond molecular dynamics (MD) simulation of αCD, in water, [69] recapitulated the multistable nature of ψ, and added a third minor ψ-state to the two inferred from NMR. These findings demonstrate the feasibility of multi-state ψ angle distributions producing C1 and C4 shifts with magnitudes similar to the Δ_{ppm} for the pirouette ON-state ([3] rotaxane).

The torsion angle dependence of the C2 shift appears to have received far less attention than C1 and C4. However, recent DFT calculations by Vila and co-workers have highlighted the torsion angle H2-C2-O2-H (i.e. rotations about C2-O2) as having an influence on C1 shifts, and raises the possibility of an effect on C2 itself [70].

In light of the αCD results above, and the general sensitivity of ^{13}C shifts to local torsion angles [71-72] , we identify the αCD C1, C2, and C4 dispersion in the pirouette-ON state ([3]rotaxane) as indicative of torsion angle fluctuations, particularly ψ, a glycosidic torsion angle defining the overall shape of the αCD macrocycle.

The C1, C2, and C4 dispersion responses could be fit to the same two-state process (i.e. same k_{EX} and P_{MIN}). We are therefore driven to speculate as to possible torsional fluctuations that would promote collective C1, C2, and C4 responses. One possibility is correlated torsion angle dynamics, such as ψ and that defined by H2-C2-O2-H. Fluctuations of ψ could be correlated with the "flip-flop" of O2 between alternative hydrogen bond configurations that differ in the rotational freedom of torsion angle, H2-C2-O2-H. Candidate hydrogen

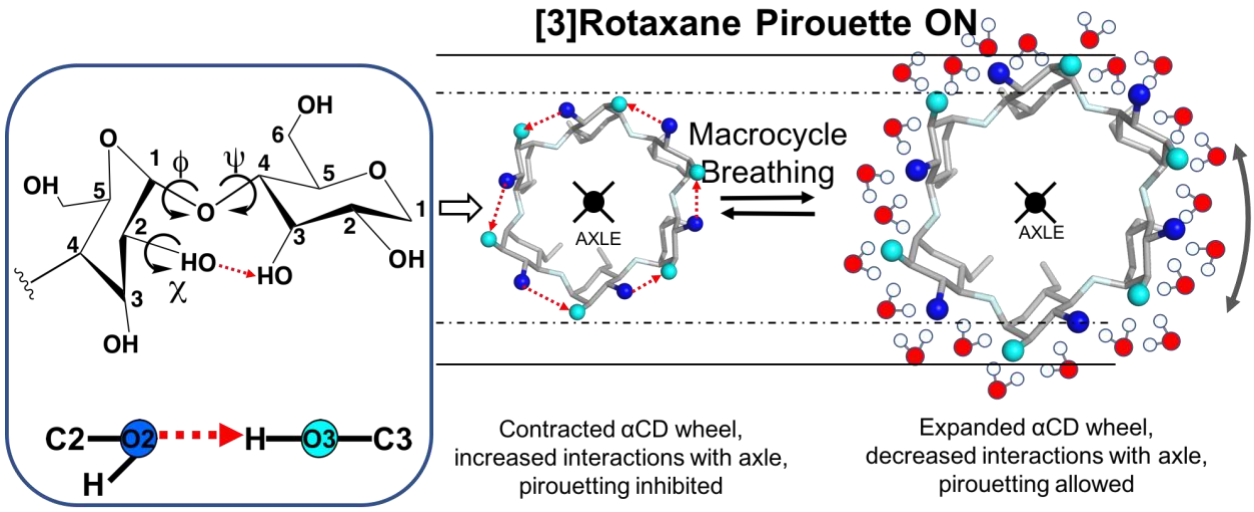

Figure 6. Macrocycle breathing model for αCD pirouette motion in ([3]rotaxane). The figure depicts one αCD wheel of [3]rotaxane, viewed along the axle axis, pirouetting about the encapsulated axle. Thermal energy fluctuations enable transient expansions of the αCD cavity which reduce non-covalent interactions with the axle to favor rotary pirouette motion. Cavity expansion involves coordinated changes in αCD glycosidic torsion angles ϕ and ψ (left box) around the wheel, which in turn disrupts hydrogen-bonds between the acceptor 2- O_1H and donor 3-O_1H in adjacent glucopyranosyl residues, and interfacial hydrogen bonds between the two αCD wheels. These hydrogen bonds experience transient disruption by solvation which is enhanced by the trace water molecules in the d6-DMSO solvent. The acceptor 2- O_1H is part of torsion angle χ (H2-C2-O2-H in the main text).

bonds include transient "intra-wheel" hydrogen-bonds within one αCD macrocycle [73], or hydrogen bonds *between* the head-to-head αCD macrocycles (**Figure 4**). However, this raises the question as to why C3, which is ostensibly similar to C2, lacks switchable ^{13}C $R_{2,CPMG}$ dispersion. The asymmetric behavior may be related to the preference for O2 acceptor hydrogen bonds over O3 acceptor hydrogen bonds noted in NMR studies of isolated αCD [74-75].

Alternatively, the collective C1, C2, and C4 responses could be due to the correlated torsion angle dynamics around the glucopyranose backbone, reported by the above-mentioned five microsecond MD simulation of αCD in H_2O [69]. Notably, the simulation revealed that transient fluctuations of the αCD cavity radius (0.05 to 0.2 nm) coincident with correlated torsion angle motions. The aforementioned "allosteric" effects of the boronate ester bonds indirectly support this type of correlated motion: these bonds to C6 of two adjacent glucopyranose residues affect the motion of carbons C1, C2, and C4 for the entire αCD macrocycle.

We note that the fitted "plateau" values, $R_{2,NE}$, for C2 and C4 (but not C1) are larger than expected based on τ_{ROT}. Higher $R_{2,NE}$ is often diagnostic of additional exchange processes with rate constants $k_{EX,FAST} > 2\pi\nu_{EFF,MAX}$, which manifest as offset on top of the rigorous $R_{2,NE}$ [41]. In the context of a two-state model, this would mean that one or both of the exchanging states identified at lower ν_{EFF} is actually two substates in rapid exchange. Exploring this possibility calls for alternative experimental methods better suited for faster time scale motions (*vide infra*).

Hydrogen bond reorganization and the effects of trace amounts of water. Dynamic hydrogen bonding (i.e. transient bond breakage/formation) is the likely origin for the 3-O_1H/2-O_1H $R_{1\rho}$ dispersion profiles observed for the pirouette-ON state ([3]rotaxane). The process would modulate the O_1H chemical shifts, and show sensitivity to OFF/ON switching. In fact, labile hydrogen bonds involving 3-O_1H donor /2-O_1H acceptor (3-O — H ····2-O) pairs have been established by both liquid-state NMR experiments [74] and MD simulations [69] in studies of isolated α–, β–, and γ-CDs. Of course, a critical difference between those studies and the present work is that our αCDs are mounted (mechanically bonded) as a head-to-head pair on an axle. Thus, the prevailing hydrogen bond network may go beyond just intra-wheel interactions to include *cross*-wheel interactions (**Figure 4**).

While the rotaxane NMR solvent was ostensibly deuterated DMSO, the samples contained trace amounts of water (mainly HDO), introduced during sample preparation which was done under open-air, bench-top conditions (in this study). These trace water molecules raise interesting possibilities for the atomic motions driving the ^1H $R_{1\rho}$ dispersion observed for the pirouette-ON state. Suppose that the hydroxyl ^1H $R_{1\rho}$ dispersion reflects the "flip-flop" of αCD 3-O_1H/2-O_1H between alternative hydrogen bond configurations (either within one or between two αCD macrocycles). Such "flip-flops" would involve transient hydrogen-bond breaking,

an event with a rate-constant (probability-per-unit-time) dictated by its corresponding activation barrier. Trace amounts of water (HDO) could lower the activation barrier, by solvating the 3-O_1H/2-O_1H hydroxyls in their "non-internally hydrogen-bonded" states. HDO-hydroxyl hydrogen bonds are considered more labile than DMSO-hydroxyl hydrogen bonds, with shorter lifetimes [76]. Hence, HDO could lower the activation barrier for hydrogen-bond reorganization, relative to neat DMSO, by providing labile, readily accessible hydrogen bond donors/acceptors for the 3-O_1H/2-O_1H hydroxyls. ^{1}H spectra of the pirouette-ON state ([3]rotaxane) prepared under different anhydrous conditions (Supporting Information, **Figure S4**) supports this hypothesis. In particular, its 3-O_1H/2- O_1H linewidths vary with the amount of residual water, suggesting that the exchange broadening scales with the water availability. Further insight could come from increasing the deuterium content (isotope effect) and observing changes (or, lack thereof) in the dispersion rate constants. Such work is in progress.

A model of switchable rotary motion. To summarize, previous literature establishes the dependence of the ^{13}C and ^{1}H chemical shifts on local torsion angles and hydrogen bond networks. Our relaxation dispersion experiments reveal time-dependent chemical shifts in the pirouette-ON ([3]rotaxane) absent in the pirouette-OFF ([1]rotaxane), and thus, indicate some form of switchable, internal motion. The motion most likely entails fluctuations of the backbone glycosidic linkages (ϕ, ψ) influencing the αCD ^{13}C methine chemical shifts, accompanied by reorganization of hydrogen-bonds that involve the 2-OH/3-OH hydroxyls. The ^{13}C and hydroxyl ^{1}H dispersion profiles are compatible with a global, two-state exchange process (same P_{Min} and k_{EX}), suggesting they partake in the same collective motion. The switchable dispersion observed at the axle CH_2 (proton 'h') appears to reflect a different dynamic process. This is plausible, considering that the axle and αCD wheels in the pirouette-ON state ([3]rotaxane) are not covalently connected, and could therefore adopt different modes of motion.

The above considerations lead us to a model for pirouette motion outlined in **Figure 6**, in which the dynamics intrinsic to the pirouette-ON state correspond to fluctuations in the αCD cavity size (i.e. inner diameter). We envision the αCD cavities sampling a distribution of inner diameter sizes, the larger sizes favoring stochastic rotary motion of the αCD wheels, and smaller sizes discouraging it. The notion that the αCD cavity diameter determines the strength of the non-covalent interactions with the encapsulated axle is well-established by the myriad of host-guest studies investigating the guest size complementarity of different CD hosts [73-74]. For the pirouette-ON state ([3]rotaxane), the methylenes of the axle component act as the encapsulated "guest". We propose that: (**i**) αCD pirouetting is favored upon reduction of non-covalent interactions between the wheel and the axle; (**ii**) Transient reduction of these interactions is a consequence of transient αCD cavity expansions resulting from thermal fluctuations in the glycosidic torsion angles (ψ in particular) *and* the 3-O_1H/2-O_1H mediated hydrogen bonds [74-75, 77-78] . (**iii**) The torsion angle and hydrogen bond fluctuations are plausible modulators of the ^{13}C and ^{1}H hydroxyl chemical shifts sensed by the ^{13}C CPMG and ^{1}H $R_{1\rho}$ relaxation dispersion experiments. A tempting speculation is that the primary degrees of freedom for breathing are correlated fluctuations of ψ and H2-C2-O2-H (χ in **Figure 6**). These torsions, found at each glycosidic linkage around the αCD wheels, could account for the compatibility of the ^{13}C and O_1H dispersion profiles with a common two-state exchange process.

In the pirouette-OFF state ([1]rotaxane) the boronate ester bonds fuse the αCD wheels to each end of the axle. Not only does this prevent each wheel from pirouetting, it brackets a glycosidic linkage and restricts its torsion angles, ϕ and ψ. Because the glucopyranose torsion angle fluctuations are correlated around the ring, the loss of torsion mobility at one glycosidic link propagates allosterically around the entire wheel. The loss of αCD backbone flexibility inhibits cavity expansion and concomitant hydrogen-bond reorganization needed for sufficient wheel/axle disengagement. The overall effect is the absence of observable relaxation dispersion throughout [1]rotaxane.

Pirouette motion in [3]rotaxane gated by transient cavity expansion/contraction is appealing for several reasons. First, it involves correlated fluctuations around the αCD wheels, which could underlie the two-state exchange process indicated by the data, with the two states being distinct clusters of wheel conformations with smaller or larger wheel cavities. Second, the trace amounts of water in the sample could render 3-O_1H/2-O_1H fluctuations more frequent by providing "lubrication" as proposed in recent computational study of facilitated rotaxane motion [79]. Our model considers the non-covalent interactions between axle and wheel as a source of internal "friction" that inhibits pirouetting of the αCD wheels. The strength of these interactions depends on the inner diameter of the αCD cavity which is modulated by thermal energy fluctuations or transient solvation of the wheel hydroxyls. Third, it offers an explanation for the pirouette-ON and OFF states showing the same τ_{ROT}, the overall rotational correlation time. In general, experimentally determined τ_{ROT} values reflect mean (conformationally averaged) shapes of the molecules in solution[34, 80]. The ON and OFF states differ in that cavity fluctuations occur freely in the ON state, but are suppressed by the boronate ester linkages in the OFF state. Critically, the cavity fluctuations sample both

larger and *smaller* diameters. Thus, the *mean* cavity sizes of the two rotaxanes are likely to be quite similar, resulting only in small changes of their diffusion tensors that remain unresolved by our methods here.

In essence, **Figure 6** proposes "macrocycle breathing" as the dynamic process gating pirouette motion in the pirouette-ON state [3]rotaxane (pirouette-ON). Such "macrocycle breathing" is conceptually similar to that observed previously in a simpler [2]rotaxane structure, where the breathing cycle modulated well-defined hydrogen binding interactions between the wheel and axle [81]. The likely non-covalent interactions within the pirouette-ON ([3]rotaxane) are dispersion interactions between the αCD cavity and the encapsulated axle methylene units, and/or polar interactions between the primary hydroxyls in the αCD tails and the functional groups at each axle end.

Caveats. The discoveries presented here raise several new questions that guide future steps in the research. First, there is evidence suggesting more rapid exchange dynamics beyond our $\nu_{EFF,MAX}$ including shallow ^{13}C dispersion observed for the 'h' methylene (**Figure 3),** and the higher $R_{2,NE}$ values for αCD C2 and C4. Strategies for accessing faster exchange include dispersion measurements at different static field strengths, adiabatic $R_{1\rho}$ or $R_{2\rho}$ measurements [30, 82], dispersion of multiple quantum coherences, varying the choice of nuclei (e.g. from ^{1}H to ^{19}F) and, of course, temperature. New information from such studies may dictate refinement of the two-state exchange parameters, such as the number and fractional population of exchange-coupled states, and the associated chemical shift differences Δ_{ppm}. That is, the two-state model and parameter values are understood to be provisional; while it has given us new insight, it is unlikely to be the final description.

At the same time, we point out that our main conclusion – the macrocycle breathing hypothesis for switchable pirouette motion, is not based on specific two-state parameter values. Instead, it is based on our discovery of an apparently cooperative exchange process, involving both ^{13}C and ^{1}H nuclei at the glycosidic linkages defining the cavity space of the αCD macrocycle, and thus, the switchable nature of its interaction with the encapsulated axle. Our macrocycle breathing hypothesis does not hinge on specific values of the model parameters used in the two-state fit.

Further tests of the macrocycle breathing hypothesis should investigate its core stipulation: exchange of the pirouette-ON state between two clusters of co-conformations that differ in the intimacy of non-covalent wheel/axle contacts. Fluctuations of these contacts could be identified by magnetization transfer between the axle and wheel components, and studies of their isolated state dynamics. In fact, we have begun ^{13}C CPMG dispersion studies of isolated αCD (Supporting Information, **Figure S5**). Our initial findings show the absence of the stark C2 dispersion exhibited by the pirouette-ON state ([3]rotaxane). Complementary studies of the axle would include investigations of its internal mobility in the isolated versus encapsulated states, and variable temperature ^{13}C dispersion measurements of the axle methylenes, analogous to those done for the methine carbons of the αCD wheels. Such studies require prior investigation of possible artifacts due to strong scalar coupling or cross-correlated ^{13}C-^{1}H dipole-dipole relaxation [83-84]. To identify distinctive features of the putative co-conformer clusters, a conventional analysis of structural parameters such as NOEs, scalar couplings, and residual-dipolar couplings, would seem inappropriate, given the extensive conformational averaging. A more appropriate approach could be a fit of the NMR parameters in terms of a conformational distribution, as demonstrated for the isolated αCD by the Widmalm and Malniak groups [68]. The potential value of including dispersion data alongside NOEs and various couplings for broader searching of multi-conformational landscapes is suggested by Ernst and co-workers in their studies of the cyclic decapeptide, antamanide [34].

The above discussion of specific mechanistic details should not obscure the broader implications of the present work: demonstration that an existing NMR method, relaxation dispersion, can provide substantial new insight into MIM motions on time scales distinct from those of standard NMR methods.

Implications of macrocycle breathing model for sliding motion. The short, fixed length of the encapsulated axle prohibits significant one-dimensional translation (sliding) of the αCD wheels along the axle length. Nevertheless, our "macrocycle breathing" model has implications for the stochastic diffusion of an αCD wheel along a long polymer chain, a central process in many poly-CD-rotaxanes including the practically important "slide-ring" polymer gels [17]. For example, a recent quasi-elastic neutron scattering (QENS) and molecular dynamics (MD) study of poly-αCD-rotaxane [85-86] by Ito and co-workers indicates that the sliding motion of αCD rings (wheels) along a long PEG axle consists of hindered "slip-stick" translational steps. Their analysis of MD trajectories included calculation of sliding motion diffusion coefficients for different inner diameters of αCD, and different simulation temperatures. Interestingly, for αCD inner diameters close to the outer diameter of the PEG axle, the calculated diffusion coefficients showed an exponential temperature dependence as depicted in our **Figure 5**. The authors linked the simulated exponential dependence to the hindered αCD sliding indicated by QENS, suggesting that it reflects diffusion over activation barriers from transient wheel/axle contacts.

Our "macrocycle breathing" model suggests an attractive mechanism to explain the hindered αCD

sliding behavior; namely, the same fluctuating non-covalent interactions between axle and wheel that gate pirouetting could also gate sliding. In this scenario, the rates of pirouetting or sliding – the two fundamental inter-component motions of all rotaxanes – are both determined by the strength of fluctuating wheel/axle contacts. If this is tenable, then our dispersion data indicate that *solvent* interactions are likely important (and controllable) factors that modulate the amplitude and time scale of these fluctuating contacts.

Conclusion. Intercomponent motion is a defining property of artificial molecular machines, either as prototypes for stand-alone nanoscale devices, or as elements within new functional materials (e.g. slip-ring polymer gels [20]). For continued advances, it is important to develop a broad portfolio of experimental techniques that can reveal physical insight and permit optimization of the motion for enhanced [87-88] performance. Biomolecular NMR spectroscopy has accrued a diverse set of experimental techniques over the last two decades for studying molecular dynamics over a broad time scale, [27, 29] but many have not yet been applied to the study of MIMs, such as the rotaxanes described here. To our knowledge, this study reports the first observation of relaxation dispersion in a MIM. Specifically, we find that ^{13}C and ^{1}H NMR relaxation dispersion measurements are consistent with a two-state exchange process for the pirouetting of αCD wheels in a [3]rotaxane with a characteristic rate constant of 2200 s^{-1} at 298 K, and a corresponding activation barrier of barrier of $\Delta F^{\ddagger} = 43 \pm 3$ kJ/mole (~ 17.4 $k_B T_R$). The exchange dynamics can be switched off by chemical conversion to a locked [1]rotaxane. A "macrocycle breathing" model is proposed to rationalize the observed exchange dynamics, in which a αCD wheel fluctuates between a contracted or expanded cavity states, the latter allowing for diffusive rotary motion about the axle. One of the mechanistic implications of this model is a possible process for stochastic diffusion of a CD wheel along a long polymer chain, a fundamental dynamic property of practically important poly-CD-rotaxanes and "slide-ring" polymer materials [85]. Relaxation dispersion is one of numerous methods in contemporary dynamic NMR that can be employed to gain site-specific descriptions of motion within MIMs over a range of time scales.

ASSOCIATED CONTENT

Supporting Information. Description of materials and sample preparation, procedures for NMR data acquisition, analysis, and model-fitting. Supporting Tables S1-S5 and Figures S1-S5, and References. The Supporting Information is available free of charge on ACS Publications website.

AUTHOR INFORMATION

Corresponding Author

*E-mail: jpeng@nd.edu

ORCID

Shannon Stoffel: 0000-0002-2636-721X
Qi-Wei Zhang: 0000-0003-1527-0559
Dong-Hao Li: 0000-0003-2556-1624
Bradley D. Smith: 0000-0003-4120-3210
Jeffrey W. Peng: 0000-0002-1226-3815

Funding Sources

This work was supported by NIH Grant R01GM059078 and NSF Grant CHE1708240 to BDS, and NIH Grant RO1GM12338 to JWP.

Notes

The authors declare no competing financial interest.

ACKNOWLEDGMENT

We are grateful to Ms Janel M. Dempsey, Ms Kayla Dempster, and Dr. Jamie van Pelt for assistance with sample preparation, data interpretation, and critical reading of the manuscript.

REFERENCES

1. Sauvage, J. P., From Chemical Topology to Molecular Machines (Nobel Lecture). *Angew Chem Int Ed Engl* **2017,** *56* (37), 11080-11093.
2. Stoddart, J. F., Mechanically Interlocked Molecules (MIMs)-Molecular Shuttles, Switches, and Machines (Nobel Lecture). *Angew Chem Int Ed Engl* **2017,** *56* (37), 11094-11125.
3. Dietrich-Buchecker, C. O.; Marnot, P. A.; Sauvage, J. P.; Kirchoff, J. R.; McMillin, D. R., Bis(2,9-diphenyl-1,10-phenanthroline) copper(I): a copper complex with a long-lived charge-transfer excited state. *Chem Commun (Camb)* **1983**, 513-514.
4. Livoreil, A.; Dietrich-Buchecker, C. O.; Sauvage, J. P., Electronically Triggered Swinging of a [2]-Catenate. *J. Am. Chem. Soc.* **1994,** *116*, 9399-9400.
5. Anelli, P. L.; Spencer, N.; Stoddart, J. F., A molecular shuttle. *J Am Chem Soc* **1991,** *113* (13), 5131-5133.
6. Zhang, Q.; Tu, Y.; Tian, H.; Zhao, Y. L.; Stoddart, J. F.; Agren, H., Working mechanism for a redox switchable molecular machine based on cyclodextrin: a free energy profile approach. *J Phys Chem B* **2010,** *114* (19), 6561-6.
7. Stoddart, J. F., The chemistry of the mechanical bond. *Chem Soc Rev* **2009,** *38* (6), 1802-20.
8. Ogino, H., RelativelyHigh-YieldSynthesesofRotaxanes.SynthesesandPropertiesofCompoundsConsistingofCyclodextrinsThreadedby , -DiaminoalkanesCoordinatedtoCobalt(III)Complexes. *J. Am. Chem. Soc.* **1981,** *103*, 1303-1304.
9. Harada, A., Cyclodextrin-based molecular machines. *Acc Chem Res* **2001,** *34* (6), 456-64.
10. Hashidzume, A.; Yamaguchi, H.; Harada, A., Cyclodextrin-Based Rotaxanes: from Rotaxanes to Polyrotaxanes and Further to Functional Materials. *Eur. J. of Org. Chem.* **2019**, 3344-3357.
11. Zhao, Y. L.; Dichtel, W. R.; Trabolsi, A.; Saha, S.; Aprahamian, I.; Stoddart, J. F., A redox-switchable alpha-cyclodextrin-based [2]rotaxane. *J Am Chem Soc* **2008,** *130* (34), 11294-6.
12. Bruns, C. J.; Frasconi, M.; Iehl, J.; Hartlieb, K. J.; Schneebeli, S. T.; Cheng, C.; Stupp, S. I.; Stoddart, J. F., Redox

switchable daisy chain rotaxanes driven by radical-radical interactions. *J Am Chem Soc* **2014,** *136* (12), 4714-23.
13. Qu, D. H.; Wang, Q. C.; Tian, H., A half adder based on a photochemically driven [2]rotaxane. *Angew Chem Int Ed Engl* **2005,** *44* (33), 5296-9.
14. Nishimura, D.; Oshikiri, T.; Takashima, Y.; Hashidzume, A.; Yamaguchi, H.; Harada, A., Relative rotational motion between alpha-Cyclodextrin Derivatives and a stiff axle molecule. *J Org Chem* **2008,** *73* (7), 2496-502.
15. Zhang, Q. W.; Zajicek, J.; Smith, B. D., Cyclodextrin Rotaxane with Switchable Pirouetting. *Org Lett* **2018,** *20* (7), 2096-2099.
16. Harada, A.; Li, J.; Kamachi, M., The molecular necklace: A rotaxane containing many threaded alpha-cyclodextrins. *Nature* **1992,** *356*, 325-327.
17. Okumura, Y.; Ito, K., The Polyrotaxane gel: A Topological gel by figure-of-eight cross-links. *Adv. Mater.* **2001,** *13*, 485-487.
18. Noda, Y.; Hayashi, Y.; Ito, K., From Topological Gels to Slide-Ring Materials. *Journal of Applied Polymer Science* **2014,** *131* (15).
19. Ito, K.; Kato, K.; Mayumi, K., *Polyrotaxane and Slide-Ring Materials*. Royal Society of Chemistry: 2016.
20. Ito, K., Slide-Ring Materials Using Cyclodextrin. *Chem Pharm Bull (Tokyo)* **2017,** *65* (4), 326-329.
21. Peng, J. W., Exposing the Moving Parts of Proteins with NMR Spectroscopy. *J Phys Chem Lett* **2012,** *3* (8), 1039-1051.
22. Gutowsky, H. S.; McCall, D. W.; Slichter, C. P., Nuclear Magnetic Resonance Multiplets in Liquids. *J. Chem. Phys.* **1953,** *21* (2), 279-292.
23. McConnell, H. M., Reaction Rates by Nuclear Magnetic Resonance. *J. Chem. Phys.* **1958,** *28* (3), 430-431.
24. Forsen, S.; Hoffman, R. A., Study of Moderately Rapid Chemical Exchange Reactions by Means of Nuclear Magnetic Double Resonance. *J. Chem. Phys.* **1963,** *39* (11), 2892-2901.
25. Stoesz, J. D.; Redfield, A. G., Cross relaxation and spin diffusion effects on the proton NMR of biopolymers in H2O. Solvent saturation and chemical exchange in superoxide dismutase. *FEBS Lett* **1978,** *91* (2), 320-4.
26. Jeener, J.; Meier, B. H.; Bachmann, P.; Ernst, R. R., Investigatoin of exchange processes by two-dimensional NMR spectroscopy. *J. Chem. Phys.* **1979,** *71* (11), 4546-4553.
27. Cavanagh, J.; Fairbrother, W. J.; Palmer III, A. G.; Rance, M.; Skelton, N. J., *Protein NMR Spectroscopy: Principles and Practice*. 2nd ed.; Academic Press: 2006; p 912.
28. Kleckner, I. R.; Foster, M. P., An introduction to NMR-based approaches for measuring protein dynamics. *Biochim Biophys Acta* **2011,** *1814* (8), 942-68.
29. Vallurupalli, P.; Sekhar, A.; Yuwen, T.; Kay, L. E., Probing conformational dynamics in biomolecules via chemical exchange saturation transfer: a primer. *J Biomol NMR* **2017,** *67* (4), 243-271.
30. Xue, Y.; Kellogg, D.; Kimsey, I. J.; Sathyamoorthy, B.; Stein, Z. W.; McBrairty, M.; Al-Hashimi, H. M., Characterizing RNA Excited States Using NMR Relaxation Dispersion. *Methods Enzymol* **2015,** *558*, 39-73.
31. Namanja, A. T.; Wang, X. D. J.; Xu, B. L.; Mercedes-Camacho, A. Y.; Wilson, B. D.; Wilson, K. A.; Etzkorn, F. A.; Peng, J. W., Toward Flexibility-Activity Relationships by NMR Spectroscopy: Dynamics of Pin1 Ligands. *Journal of the American Chemical Society* **2010,** *132* (16), 5607-+.
32. Gutowsky, H. S.; Vold, R. L.; Wells, E. J., Theory of Chemical Exchange Effects in Magnetic Resonance. *The Journal of Chemical Physics* **1965,** *43* (11), 4107-4125.
33. Deverell, C.; Morgan, R. E.; Strange, J. H., Studies of Chemical Exchange by Nuclear Magnetic Relaxation in Rotating Frame. *Molecular Physics* **1970,** *18* (4), 553-&.
34. Blackledge, M. J.; Bruschweiler, R.; Griesinger, C.; Schmidt, J. M.; Xu, P.; Ernst, R. R., Conformational Backbone Dynamics of the Cyclic Decapeptide Antamanide - Application of a New Multiconformational Search Algorithm-Based on Nmr Data. *Biochemistry* **1993,** *32* (41), 10960-10974.
35. Millet; Loria, J. P.; Kroenke, C. D.; Pons, M.; Palmer, A. G., The Static Magnetic Field Dependence of Chemical Exchange Linebroadening Defines the NMR Chemical Shift Time Scale. *J Am Chem Soc* **2000,** *122* (12), 2867-2877.
36. Deverell, C.; Morgan, R. E.; Strange, J. H., Studies of chemical exchange by nuclear magnetic relaxation in the rotating frame. *Molecular Physics* **1970,** *18* (4), 553-559.
37. Wennerstrom, H., Nuclear Magnetic-Relaxation Induced by Chemical Exchange. *Molecular Physics* **1972,** *24* (1), 69-+.
38. Carver, J. P.; Richards, R. E., A general two-site solution for the chemical exchange produced dependence of T2 upon the carr-Purcell pulse separation. **1972,** *6* (1), 89-105.
39. Mulder, F. A. A.; Mittermaier, A.; Hon, B.; Dahlquist, F. W.; Kay, L. E., Studying excited states of proteins by NMR spectroscopy. **2001,** *8* (11), 932-935.
40. Zintsmaster, J. S.; Wilson, B. D.; Peng, J. W., Dynamics of ligand binding from 13C NMR relaxation dispersion at natural abundance. *J Am Chem Soc* **2008,** *130* (43), 14060-1.
41. Palmer, A. G., 3rd; Kroenke, C. D.; Loria, J. P., Nuclear magnetic resonance methods for quantifying microsecond-to-millisecond motions in biological macromolecules. *Methods Enzymol* **2001,** *339*, 204-38.
42. Nirmala, N. R.; Wagner, G., Measurement of 13C relaxation times in proteins by two-dimensional heteronuclear 1H-13C correlation spectroscopy. *Journal of the American Chemical Society* **1988,** *110* (22), 7557-7558.
43. Palmer, A. G.; Rance, M.; Wright, P. E., Intramolecular motions of a zinc finger DNA-binding domain from Xfin characterized by proton-detected natural abundance carbon-13 heteronuclear NMR spectroscopy. *Journal of the American Chemical Society* **1991,** *113* (12), 4371-4380.
44. Gibbs, S. J.; Johnson, C. S., A Pfg Nmr Experiment for Accurate Diffusion and Flow Studies in the Presence of Eddy Currents. *Journal of Magnetic Resonance* **1991,** *93* (2), 395-402.
45. Berg, H. C., *Random Walks in Biology*. Princeton University Press: 1993; p 152.
46. Dalvit, C.; Hommel, U., Sensitivity-Improved Detection of Protein Hydration and Its Extension to the Assignment of Fast-Exchanging Resonances. *J. Magn. Reson. Ser. B* **1995,** *109*, 334-338.
47. Dalvit, C., New One-Dimensional Selective NMR Experiments in Aqueous Solutions Recorded with Pulsed Field Gradients. *J. Magn. Reson. Ser. A* **1995,** *113*, 120-123.
48. Trott, O.; Palmer, A. G., R1ρ Relaxation outside of the Fast-Exchange Limit. **2002,** *154* (1), 157-160.
49. Arrhenius, S., Ueber die Reaktionsgeschwindigkeit bei der Inversion von Rohrzucker durch Saeuren. *Zeitschrift fuer Physikalische Chemie* **1889,** *4* (1), 226-248.
50. Oh, K.-I.; Baiz, C. R., Crowding Stabilizes DMSO–Water Hydrogen-Bonding Interactions. *The Journal of Physical Chemistry B* **2018,** *122* (22), 5984-5990.
51. Bissell, R. A.; Cordova, E.; Kaifer, A. E.; Stoddart, J. F., A Chemically and Electrochemically Switchable Molecular Shuttle. *Nature* **1994,** *369* (6476), 133-137.
52. Pons, M.; Millet, O., Dynamic NMR studies of supramolecular complexes. *Progress in Nuclear Magnetic Resonance Spectroscopy* **2001,** *38* (4), 267-324.
53. Nygaard, S.; Leung, K. C.; Aprahamian, I.; Ikeda, T.; Saha, S.; Laursen, B. W.; Kim, S. Y.; Hansen, S. W.; Stein, P. C.; Flood, A. H.; Stoddart, J. F.; Jeppesen, J. O., Functionally rigid bistable [2]rotaxanes. *J Am Chem Soc* **2007,** *129* (4), 960-70.
54. Lee, C. F.; Leigh, D. A.; Pritchard, R. G.; Schultz, D.; Teat, S. J.; Timco, G. A.; Winpenny, R. E., Hybrid organic-inorganic rotaxanes and molecular shuttles. *Nature* **2009,** *458* (7236), 314-8.
55. Gao, C.; Luan, Z. L.; Zhang, Q.; Yang, S.; Rao, S. J.; Qu, D. H.; Tian, H., Triggering a [2]Rotaxane Molecular Shuttle by a Photochemical Bond-Cleavage Strategy. *Org Lett* **2017,** *19* (7), 1618-1621.
56. Zhu, K.; Baggi, G.; Loeb, S. J., Ring-through-ring molecular shuttling in a saturated [3]rotaxane. *Nat Chem* **2018,** *10* (6), 625-630.
57. Changeux, J. P., Allostery and the Monod-Wyman-Changeux model after 50 years. *Annu Rev Biophys* **2012,** *41*, 103-33.

58. Boulton, S.; Melacini, G., Advances in NMR Methods To Map Allosteric Sites: From Models to Translation. *Chem Rev* **2016,** *116* (11), 6267-304.
59. Wodak, S. J.; Paci, E.; Dokholyan, N. V.; Berezovsky, I. N.; Horovitz, A.; Li, J.; Hilser, V. J.; Bahar, I.; Karanicolas, J.; Stock, G.; Hamm, P.; Stote, R. H.; Eberhardt, J.; Chebaro, Y.; Dejaegere, A.; Cecchini, M.; Changeux, J. P.; Bolhuis, P. G.; Vreede, J.; Faccioli, P.; Orioli, S.; Ravasio, R.; Yan, L.; Brito, C.; Wyart, M.; Gkeka, P.; Rivalta, I.; Palermo, G.; McCammon, J. A.; Panecka-Hofman, J.; Wade, R. C.; Di Pizio, A.; Niv, M. Y.; Nussinov, R.; Tsai, C. J.; Jang, H.; Padhorny, D.; Kozakov, D.; McLeish, T., Allostery in Its Many Disguises: From Theory to Applications. *Structure* **2019,** *27* (4), 566-578.
60. Dudley, R. L.; Fyfe, C. A.; Stephenson, P. J.; Deslandes, Y.; Hamer, G. K.; Marchessault, R. H., High-Resolution C-13 Cp/Mas Nmr-Spectra of Solid Cellulose Oligomers and the Structure of Cellulose-Ii. *Journal of the American Chemical Society* **1983,** *105* (8), 2469-2472.
61. Saito, H., Conformation-Dependent C-13 Chemical-Shifts - a New Means of Conformational Characterization as Obtained by High-Resolution Solid-State C-13 Nmr. *Magnetic Resonance in Chemistry* **1986,** *24* (10), 835-852.
62. Gidley, M. J.; Bociek, S. M., C-13 Cp/Mas Nmr-Studies of Amylose Inclusion Complexes, Cyclodextrins, and the Amorphous Phase of Starch Granules - Relationships between Glycosidic Linkage Conformation and Solid-State C-13 Chemical-Shifts. *Journal of the American Chemical Society* **1988,** *110* (12), 3820-3829.
63. Jarvis, M. C., Relationship of Chemical-Shift to Glycosidic Conformation in the Solid-State C-13 Nmr-Spectra of (1-]4)-Linked Glucose Polymers and Oligomers - Anomeric and Related Effects. *Carbohydrate Research* **1994,** *259* (2), 311-318.
64. Manor, P. C.; Saenger, W., Water Molecule in Hydrophobic Surroundings - Structure of Alpha-Cyclodextrin-Hexahydrate (C6h10o5)6.6h2o. *Nature* **1972,** *237* (5355), 392-&.
65. Manor, P. C.; Saenger, W., Topography of Cyclodextrin Inclusion Complexes .3. Crystal and Molecular-Structure of Cyclohexaamylose Hexahydrate, (H2o)2 Inclusion Complex. *Journal of the American Chemical Society* **1974,** *96* (11), 3630-3639.
66. O'Brien, E. P.; Moyna, G., Use of 13C chemical shift surfaces in the study of carbohydrate conformation. Application to cyclomaltooligosaccharides (cyclodextrins) in the solid state and in solution. **2004,** *339* (1), 87-96.
67. Sergeyev, I.; Moyna, G., Determination of the three-dimensional structure of oligosaccharides in the solid state from experimental 13C NMR data and ab initio chemical shift surfaces. *Carbohydr Res* **2005,** *340* (6), 1165-74.
68. Thaning, J.; Stevensson, B.; Östervall, J.; Naidoo, K. J.; Widmalm, G.; Maliniak, A., NMR Studies of Molecular Conformations in α-Cyclodextrin. *The Journal of Physical Chemistry B* **2008,** *112* (29), 8434-8436.
69. Suárez, D.; Díaz, N., Conformational and entropy analyses of extended molecular dynamics simulations of α-, β- and γ-cyclodextrins and of the β-cyclodextrin/nabumetone complex. *Physical Chemistry Chemical Physics* **2017,** *19* (2), 1431-1440.
70. Garay, P. G.; Martin, O. A.; Scheraga, H. A.; Vila, J. A., Factors Affecting the Computation of the C-13 Shielding in Disaccharides. *Journal of Computational Chemistry* **2014,** *35* (25), 1854-1864.
71. de Dios, A. C.; Pearson, J. G.; Oldfield, E., Secondary and tertiary structural effects on protein NMR chemical shifts: an ab initio approach. *Science* **1993,** *260* (5113), 1491-6.
72. Williamson, M. P., Using chemical shift perturbation to characterise ligand binding. *Prog Nucl Magn Reson Spectrosc* **2013,** *73*, 1-16.
73. Saenger, W.; Jacob, J.; Gessler, K.; Steiner, T.; Hoffmann, D.; Sanbe, H.; Koizumi, K.; Smith, S. M.; Takaha, T., Structures of the Common Cyclodextrins and Their Larger AnaloguesBeyond the Doughnut. *Chemical Reviews* **1998,** *98* (5), 1787-1802.
74. Schneider, H. J.; Hacket, F.; Rudiger, V.; Ikeda, H., NMR Studies of Cyclodextrins and Cyclodextrin Complexes. *Chem Rev* **1998,** *98* (5), 1755-1786.
75. Naidoo, K. J.; Gamieldien, M. R.; Chen, J. Y.; Widmalm, G.; Maliniak, A., Glucose orientation and dynamics in alpha-, beta-, and gamma-cyclodextrins. *J Phys Chem B* **2008,** *112* (47), 15151-7.
76. Luzar, A.; Chandler, D., Structure and Hydrogen-Bond Dynamics of Water-Dimethyl Sulfoxide Mixtures by Computer-Simulations. *J. Chem. Phys.* **1993,** *98* (10), 8160-8173.
77. Saenger, W.; Noltemeyer, M.; Manor, P. C.; Hingerty, B.; Klar, B., Topography of Cyclodextrin Inclusion Compounds .9. Induced-Fit-Type Complex-Formation of Model Enzyme Alpha-Cyclodextrin. *Bioorganic Chemistry* **1976,** *5* (2), 187-195.
78. Suarez, D.; Diaz, N., Conformational and entropy analyses of extended molecular dynamics simulations of alpha-, beta- and gamma-cyclodextrins and of the beta-cyclodextrin/nabumetone complex. *Phys Chem Chem Phys* **2017,** *19* (2), 1431-1440.
79. Fu, H.; Shao, X.; Chipot, C.; Cai, W., The lubricating role of water in the shuttling of rotaxanes. *Chem Sci* **2017,** *8* (7), 5087-5094.
80. Abragam, A., *The Principles of Nuclear Magnetism*. Clarendon Press, Oxford: 1961; p 599.
81. Murgu, I.; Baumes, J. M.; Eberhard, J.; Gassensmith, J. J.; Arunkumar, E.; Smith, B. D., Macrocycle breathing in [2]rotaxanes with tetralactam macrocycles. *J Org Chem* **2011,** *76* (2), 688-91.
82. Palmer, A. G., 3rd; Massi, F., Characterization of the dynamics of biomacromolecules using rotating-frame spin relaxation NMR spectroscopy. *Chem Rev* **2006,** *106* (5), 1700-19.
83. Fagerness, P. E.; Grant, D. M.; Kuhlmann, K. F.; Mayne, C. L.; Parry, R. B., Spin-Lattice Relaxation in Coupled 3 Spin Systems of Ais Type. *Journal of Chemical Physics* **1975,** *63* (6), 2524-2532.
84. Daragan, V. A.; Mayo, K. H., Tri- and diglycine backbone rotational dynamics investigated by 13C NMR multiplet relaxation and molecular dynamics simulations. *Biochemistry* **1993,** *32* (43), 11488-99.
85. Yasuda, Y.; Hidaka, Y.; Mayumi, K.; Yamada, T.; Fujimoto, K.; Okazaki, S.; Yokoyama, H.; Ito, K., Molecular Dynamics of Polyrotaxane in Solution Investigated by Quasi-Elastic Neutron Scattering and Molecular Dynamics Simulation: Sliding Motion of Rings on Polymer. *J Am Chem Soc* **2019,** *141* (24), 9655-9663.
86. Yasuda, Y.; Toda, M.; Mayumi, K.; Yokoyama, H.; Morita, H.; Ito, K., Sliding Dynamics of Ring on Polymer in Rotaxane: A Coarse-Grained Molecular Dynamics Simulation Study. *Macromolecules* **2019,** *52* (10), 3787-3793.
87. Bodis, P.; Panman, M. R.; Bakker, B. H.; Mateo-Alonso, A.; Prato, M.; Buma, W. J.; Brouwer, A. M.; Kay, E. R.; Leigh, D. A.; Woutersen, S., Two-Dimensional Vibrational Spectroscopy of Rotaxane-Based Molecular Machines. *Accounts of Chemical Research* **2009,** *42* (9), 1462-1469.
88. Panman, M. R.; van Dijk, C. N.; Huerta-Viga, A.; Sanders, H. J.; Bakker, B. H.; Leigh, D. A.; Brouwer, A. M.; Buma, W. J.; Woutersen, S., Transient two-dimensional vibrational spectroscopy of an operating molecular machine. *Nature Communications* **2017,** *8*.

For Table of Contents Only

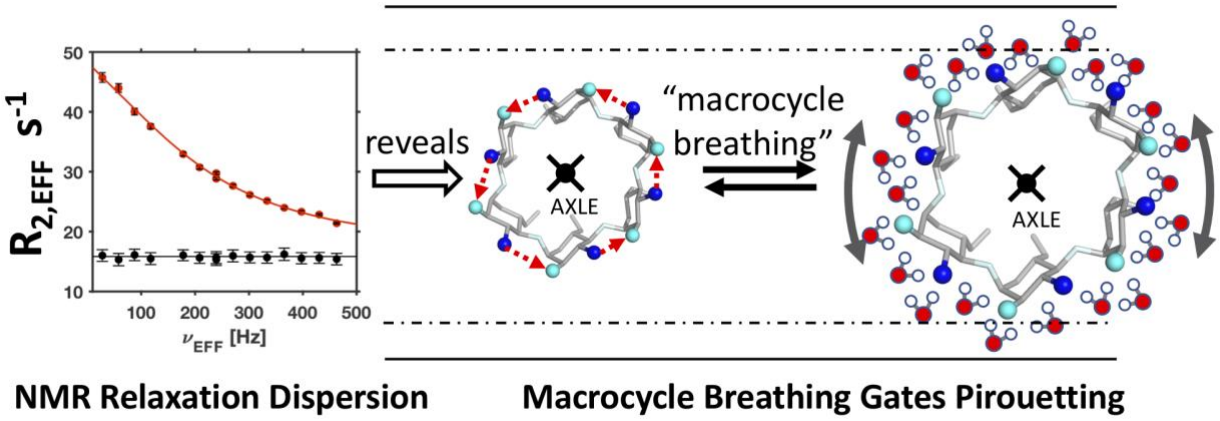

NMR Relaxation Dispersion **Macrocycle Breathing Gates Pirouetting**